Scattering-angle dependence of doubly differential cross sections for ionization in proton collisions with molecular hydrogen

C. T. Plowman [1,*] K. H. Spicer [1] M. Schulz,[2] and A. S. Kadyrov [1,3]

[1]*Department of Physics and Astronomy, Curtin University, GPO Box U1987, Perth, Western Australia 6845, Australia*

[2]*Physics Department and LAMOR, Missouri University of Science & Technology, Rolla, Missouri 65409, USA*

[3]*Institute of Nuclear Physics, Ulugbek, 100214 Tashkent, Uzbekistan*

(Received 6 July 2023; accepted 17 October 2023; published 9 November 2023)

The wave-packet convergent close-coupling (WP-CCC) approach is applied to calculate the energy spectrum of electrons ejected in $p + H_2$ collisions as a function of the scattering angle of the projectile. The calculations are performed for projectile energies of 75, 100, and 200 keV. At these incident energies there are many competing reaction channels that play an essential role in the collision dynamics. The target is modeled as an orientationally averaged effective one-electron system. The results are compared with available perturbative calculations and experimental data. Good agreement between the WP-CCC results and experimental data is found for small emission energies, especially when the projectile is scattered at small angles. However, when the electron is emitted with a speed comparable to or greater than the projectile speed we find that our method predicts smaller cross sections near zero scattering angles and a slower fall off than the experimental data. This is in agreement with other calculations. Furthermore, the structure observed in the experimental data at large scattering angles is not supported by our results. Interestingly, we find very good agreement with the continuum-distorted-wave eikonal-initial-state molecular-orbital calculations that use a two-effective center approximation, though our method describes the target as an effective one-electron spherically symmetric system. This suggests that in these models two-center interference effects may have a small effect on this particular cross section. Furthermore, we find that the experimentally observed decrease in average scattering angle in proton collisions with H_2 near the electron-projectile matching speed is not reproduced by our results. We also present the doubly differential cross section for ionization as a function of the scattering angle of the projectile at select emission angles.

DOI: 10.1103/PhysRevA.108.052809

I. INTRODUCTION

Collisions between ions, atoms, and molecules remains an active area of research. The complexity of collision systems with more than two charged particles has presented a significant challenge towards developing a complete theory capable of accurately describing many possible scattering outcomes across a wide range of incident energies. For a review of the most recent developments and progress in the field of ion-atom and ion-molecule collisions, see Refs. [1,2]. In addition, experimental measurements can be very challenging for some collision processes. However, accurate collision data for many simple and complex scattering systems is required for a number of practical applications. Very accurate cross sections are needed for a vast number of projectile and target species for plasma diagnostics and neutral beam heating used in nuclear fusion [3–5], interpretation of x-ray spectra from extraterrestrial sources [6,7], and Monte Carlo simulations used for treatment planning in hadron therapy [8–10].

One of the most detailed observables in scattering systems is the fully differential cross section (FDCS). Due to recent advances in experimental techniques, in particular, the development of cold target recoil ion momentum spectroscopy (COLTRIMS), it has become possible to perform kinematically complete experiments that are capable of extracting the necessary information to determine the FDCS [11,12]. This has resulted in a renewed interest in proton collisions with helium and molecular hydrogen, the simplest two-electron atomic and molecular targets. These scattering systems provide a useful testing ground for theoretical advances due to their relatively simple structure. Moreover, the presence of structures attributed to potential two-centre interference effects in $p + H_2$ collisions are not fully understood and require further development of theoretical techniques [13–15]. The recent measurements of the FDCS for single ionization in $p + H_2$ collisions have highlighted shortcomings in currently available theoretical methods which give results that are significantly different from the experimental data [16]. Discrepancies between theory and experiment are also present for measurements of dissociative electron capture [15,17]. These experiments demonstrate the deficiencies of the theoretical approaches commonly used for calculating less detailed integrated total and singly differential cross sections when the later applied to more detailed fully differential cross sections.

Many methods have been developed to model ion-atom collisions. At low incident energies where the probability of ionization is relatively small, molecular-orbital close-coupling [18] and adiabatic hyperspherical [19] methods are capable of providing accurate integrated cross sections. On the

*corey.plowman@postgrad.curtin.edu.au

other hand, for sufficiently energetic projectiles, perturbative methods such as those based on the Born series expansion and continuum-distorted-wave (CDW) methods can accurately predict the various scattering outcomes [20]. The most theoretically challenging energy region lies between these two extremes, where the total cross section for ionization peaks and many open reaction channels are strongly interconnected. A number of approaches have been developed to tackle intermediate-energy ion-atom collisions. Methods based on direct solution of the time-dependent Schrödinger equation for the scattering system are highly accurate but extremely demanding computationally. Alternative methods use the close-coupling formalism based on expanding the electronic scattering wave function in terms of atomic orbitals. The choice of basis is very important in these methods as the convergence of the results depends heavily on the type of basis functions. The accuracy of the ionization energy of the ground state is known to significantly affect the results. Furthermore, close-coupling methods were traditionally restricted to modeling collisions that do not result in ionization due to the fact that the continuum is non-square-integrable.

An alternative approach to ion-atom collisions is the classical trajectory Monte Carlo (CTMC) method [21]. This method is based on solving the classical equations of motion for a large number of simulated collisions and recovering cross sections from the resulting statistics. It is applicable over a wide energy range. It has been extended to multielectron targets such as He and H_2 [22–24]. However, to our best knowledge, the CTMC method has not been applied to doubly differential ionization in $p + H_2$ collisions.

While the aforementioned theoretical approaches are well suited to calculating total cross sections within the energy regimes in which they are applicable, the differential cross sections (DCS) represent a more difficult challenge. Angular differential cross sections for direct scattering and electron capture include additional information about the scattering angle dependence of the projectile, and differential cross sections for single-electron ionization can depend on up to five variables simultaneously. As a result, calculating DCS is a stringent test for theoretical methods, and most approaches have only been applied to calculate the total cross sections or certain types of DCS. Combined with the fact that most collision theories have been developed to tackle scattering on atomic targets this means there are very few accurate calculations of the DCS for ionization in proton collisions with molecular hydrogen. Typically, cross sections for atomic hydrogen are simply scaled to represent results for the molecular target.

In this work we consider the doubly differential cross section (DDCS) for ionization in proton collisions with H_2. Previously, we calculated the DDCS as a function of the energy and angle of the ejected electron, providing the first accurate description of the experimental data [25]. Details of the approach to calculating the energy and angular spectrum of electrons are given in Ref. [26]. Here we consider the DDCS as a function of the projectile scattering angle and electron energy, as well as the DDCS as a function of the projectile scattering angle and electron emission angle. The DDCS for ionization as a function of the scattering angle of the projectile and emission energy of the ejected electron was first measured experimentally by Alexander *et al.* [27] at six different emission energies for 75-keV protons incident on H_2. The energy resolution of their apparatus was ± 1.5 eV and the upper limit on the angular precision was ± 50 μrad. Their data suggest the presence of some structure in the cross section around a scattering angle of 1.4 mrad at some emission energies considered. The authors attributed this to interference resulting from the indistinguishability of which target proton the scattered wave develops from. A further study was undertaken by Egodapitiya *et al.* [28] for the single emission energy of 14.6 eV. The uncertainty in the measured scattering angle was estimated to be 0.1 mrad full width at half maximum (FWHM) and the energy resolution was 3-eV FWHM. The results slightly underestimate the data of Ref. [27]. The most recent experimental measurements of this cross section were performed by Sharma *et al.* [13]. Compared to the data from Refs. [27,28], background signals were reduced, potentially increasing the accuracy, especially at the larger scattering angles where the cross section is small. The energy resolution was estimated to be 3-eV FWHM and the scattering angle resolution was 0.15-mrad FWHM. Unlike the other experimental data, the measurements by Sharma *et al.* [13] fall off smoothly at large scattering angles and show no evidence of additional structure in the DDCS. However, a pronounced structure was reported in the coherent to incoherent ratio at about the same angle as in the DDCS of Refs. [27,28].

Theoretically, the DDCS as a function of scattering angle at fixed emission energies has been investigated with perturbative approaches. The continuum-distorted-wave eikonal-initial-state (CDW-EIS) approach to $p + H$ collisions was used by Alexander *et al.* [27] by introducing a two-center interference factor to apply the results to the molecular target. The results agree well with their experimental data at the lowest emission energies, but significant discrepancies are observed as the emission energy increases. Chowdhury *et al.* [29] used a different variation of the CDW method called the molecular three-body distorted-wave-eikonal initial-state (M3DW-EIS) approach. In this formulation the molecular target is represented by orientation-averaged electronic wave functions [30], rather than averaging the orientation-dependent cross sections over all possible orientations of the molecule as is commonly done for diatomic molecular targets [31]. Quantitatively, the results were found to consistently underestimate the experimental data of Alexander *et al.* [27], but demonstrated improved agreement in shape compared to the previously available CDW-EIS results. The first-order Born approximation (FBA) was also used by Chowdhury *et al.* [29] to calculate the same DDCS. This is the simplest perturbative method applied to the problem. The results significantly differ from the experimental data and all other calculations. The continuum-distorted-wave eikonal-initial-state molecular-orbital (CDW-EIS-MO) approximation was used by Igarashi and Gulyás [32] to investigate the DDCS for ionization in proton collisions with H_2. They used a number of different approximations to represent the interaction potential between the projectile nucleus and residual target ion, resulting in significant differences between their various calculations. To account for the two-center nature of the target nucleus they employ a two-effective center (TEC) approximation. This approach treats the target as two independent

hydrogen-like atoms separated by the equilibrium internuclear distance of H_2. They compared their results to those for the $p + H$ collision system, i.e., without the interference factor arising from the way in which they model the nuclei of the molecular target. Overall, it is seen that the inclusion of the two-center factor does not significantly alter the shape of the DDCS. None of the versions of the CDW-EIS-MO method used by Igarashi and Gulyás [32] indicated any presence of the structure seen at large scattering angles in the data of Alexander *et al.* [27]. In fact, changing the approximation used to represent the so-called postcollisional interaction has the largest effect on their results, not the introduction of the classical two-center factor. Overall the calculations demonstrated mixed agreement with experiment. As with the other CDW results, the agreement is best for low emission energies and worst at the highest emission energy considered. The various forms of heavy-particle interaction potential result in small but significant differences between their results, but no particular choice demonstrates significant improvement over the others.

We developed a nonperturbative approach to ion-atom [33–35] collisions called the wave-packet convergent close-coupling (WP-CCC) method that is capable of describing all single-electron processes with a high level of accuracy across the entire intermediate energy region. This two-center method accounts for the strong coupling between all reaction channels and is capable of handling large target- and projectile-centered bases to ensure that all significant channels are included in the calculation. Furthermore, the electron continuum is included in the theory through the construction of stationary wave packets constructed from the continuum-wave solution. The latter form a square-integrable basis of continuum pseudostates that are orthogonal to the bound eigenstates [36]. Combined with highly efficient GPU codes [37] this has positioned the WP-CCC method to tackle some of the most challenging problems in the field of ion-atom collisions.

The WP-CCC method was recently extended to treat proton collisions with molecular hydrogen [38]. Results for the total cross sections for all single-electron processes demonstrated excellent agreement with experimental data where available. The angular cross sections for direct scattering and electron capture also agreed well with the available experimental data and other theoretical methods in the literature. Significant improvement over previously available calculations was observed for the singly differential cross section for ionization [39]. Then we considered doubly differential cross sections for ionization as a function of the energy and angle of the ejected electron [25]. The WP-CCC method was found to accurately reproduce the experimental data across the entire range of electron kinematics, where available. Significant improvement over the previously available perturbative calculations was observed. In this paper we focus on the remaining two types of doubly differential cross sections for ionisation: namely, those differential in the solid angle of the projectile and energy of the ejected electron, and differential in the scattering angle of the projectile and electron-emission angle. As far as we are aware, there are no experimental measurements or theoretical calculations of the doubly differential cross section for ionization as a function of both the projectile scattering angle and emission angle of the ejected electron. Here we present results for this cross section for completeness. First we give a brief overview of the relevant aspects of the theory. Full details of the approach to differential cross sections for ionization are available in Refs. [33,40].

Unless specified otherwise, atomic units (a.u.) are used throughout this paper.

II. TWO-CENTER WAVE-PACKET CONVERGENT CLOSE-COUPLING METHOD

The WP-CCC method is described in detail in our earlier works [33,34,36,41]. The wave-packet-based approach for calculating differential cross sections for ionization was introduced in Ref. [36], and extended to positively charged projectiles in Ref. [33]. Multielectron atomic targets were considered in Refs. [37,42]. The molecular hydrogen target structure was incorporated into the WP-CCC method in Ref. [38], and singly differential cross sections were calculated in Ref. [39]. The doubly differential cross section for ionization as a function of the energy and emission angle of the ejected electron was presented in Ref. [25]. Here we give a brief overview of the relevant aspects of the WP-CCC method to calculating doubly differential cross sections as a function of the scattering angle of the projectile and energy or angle of the ejected electron.

The nonrelativistic time-independent Schrödinger equation for the total scattering wave function Ψ_i^+, subject to the outgoing-wave boundary conditions, is written as

$$(H - E)\Psi_i^+ = 0, \tag{1}$$

where H is the full three-body Hamiltonian of the collision system and E is the total energy. Subscript i refers to the initial channel from which the total scattering wave develops. In this work we consider scattering from the ground electronic state. The impact-parameter close-coupling formalism is based on expanding the total scattering wave function in terms of a set of target-centered and projectile-centered pseudostates, which we label as ψ_α and ψ_β, respectively. Hence, the total scattering wave function is given by

$$\Psi_i^+ \approx \sum_{\alpha=1}^{N} F_\alpha(t, \boldsymbol{b})\psi_\alpha(\boldsymbol{r}_\mathrm{T})\mathrm{e}^{i\boldsymbol{q}_\alpha\cdot\boldsymbol{\rho}} + \sum_{\beta=1}^{M} G_\beta(t, \boldsymbol{b})\psi_\beta(\boldsymbol{r}_\mathrm{P})\mathrm{e}^{i\boldsymbol{q}_\beta\cdot\boldsymbol{\sigma}}, \tag{2}$$

where $F_\alpha(t, \boldsymbol{b})$ and $G_\beta(t, \boldsymbol{b})$ are expansion coefficients that depend on time t and impact parameter $\boldsymbol{b}$. We use two sets of Jacobi coordinates. The first set consists of the position of the active electron relative to the target nucleus $\boldsymbol{r}_\mathrm{T}$, and the position of the projectile relative to the target system, $\boldsymbol{\rho}$. In the second set of coordinates the position of the active electron relative to the projectile nucleus is $\boldsymbol{r}_\mathrm{P}$, and the position of the residual target ion relative to the atom formed by the projectile is $\boldsymbol{\sigma}$.

The momentum of the projectile nucleus relative to the target is denoted as $\boldsymbol{q}_\alpha$, and the momentum of the residual target ion relative to the projectile atom as $\boldsymbol{q}_\beta$. The target nucleus is fixed at the origin, and the projectile moves in a straight line parallel to the z axis at an impact parameter $\boldsymbol{b}$, according to $\boldsymbol{R} = \boldsymbol{b} + \boldsymbol{v}t$, where $\boldsymbol{b} \cdot \boldsymbol{v} = 0$.

The two-center expansion in Eq. (2) ensures that electron capture into bound states of the projectile atom and ionization into the projectile continuum processes are coupled with the direct channels. This also allows us to explicitly differentiate between electron capture and ionization in the asymptotic state. The number of basis states used in the expansion is increased until the results of interest converge. Substituting Eq. (2) into Eq. (1) we obtain a set of coupled first-order differential equations for the expansion coefficients

$$\begin{aligned} i\dot{F}_{\alpha'} + i\sum_{\beta=1}^{M}\dot{G}_\beta \tilde{K}_{\alpha'\beta} &= \sum_{\alpha=1}^{N} F_\alpha D_{\alpha'\alpha} + \sum_{\beta=1}^{M} G_\beta \tilde{Q}_{\alpha'\beta}, \\ i\sum_{\alpha=1}^{N}\dot{F}_\alpha K_{\beta'\alpha} + i\dot{G}_{\beta'} &= \sum_{\alpha=1}^{N} F_\alpha Q_{\beta'\alpha} + \sum_{\beta=1}^{M} G_\beta \tilde{D}_{\beta'\beta}, \\ \alpha' = 1, 2, \ldots, N, \quad \beta' &= 1, 2, \ldots, M. \end{aligned} \tag{3}$$

Here the dots over F_α and G_β denote time derivatives, $D_{\alpha'\alpha}$ are the direct-scattering matrix elements, $K_{\beta'\alpha}$ are the overlap integrals, and $Q_{\beta'\alpha}$ are the exchange matrix elements. The tildes denote the quantities in the projectile center. In the limit as $t \to +\infty$ the expansion coefficients, $F_\alpha(t, \boldsymbol{b})$ and $G_\beta(t, \boldsymbol{b})$, yield the scattering amplitudes for the final channels α and β, respectively. Conversely, in the limit as $t \to -\infty$ they satisfy the initial boundary condition

$$\begin{aligned} F_\alpha(-\infty, \boldsymbol{b}) &= \delta_{\alpha i}, \quad \alpha = 1, 2, \ldots, N, \\ G_\beta(-\infty, \boldsymbol{b}) &= 0, \quad \beta = 1, 2, \ldots, M, \end{aligned} \tag{4}$$

i.e., in the initial channel the active electron is in the ground state of the target.

The two types of doubly differential cross section considered in this work are obtained from integrating the FDCS for ionisation according to

$$\frac{\mathrm{d}^2\sigma^{\mathrm{ion}}}{\mathrm{d}E_\mathrm{e}\mathrm{d}\Omega_f} = \int \frac{\mathrm{d}^3\sigma^{\mathrm{ion}}}{\mathrm{d}E_\mathrm{e}\mathrm{d}\Omega_\mathrm{e}\mathrm{d}\Omega_f}\mathrm{d}\Omega_e, \tag{5}$$

and

$$\frac{\mathrm{d}^2\sigma^{\mathrm{ion}}}{\mathrm{d}\Omega_\mathrm{e}\mathrm{d}\Omega_f} = \int \frac{\mathrm{d}^3\sigma^{\mathrm{ion}}}{\mathrm{d}E_\mathrm{e}\mathrm{d}\Omega_\mathrm{e}\mathrm{d}\Omega_f}\mathrm{d}E_\mathrm{e}. \tag{6}$$

In Eqs. (5) and (6), f denotes the final state after scattering, E_e is the energy of the ionized electron, Ω_e is the solid angle into which the ionized electron is emitted, and Ω_f is the solid angle that the projectile is scattered into.

The WP-CCC approach to calculating differential cross sections for ionization in proton collisions with H_2 is explained in detail in Ref. [39]. Following the idea outlined by Kadyrov *et al.* [43], the ionization amplitude is found from the postform of the Coulomb breakup amplitude given in Ref. [44]. After projecting the positive-energy pseudostates onto the true Coulomb scattering wave function the ionization amplitude is split into two parts. The first term is called direct ionisation (DI) and corresponds to ionization resulting in the ejection of the active electron in the vicinity of the target. It is given in terms of the amplitudes for excitation into the positive-energy pseudostates, $T_{fi}^{\mathrm{DS}}(\boldsymbol{q}_f, \boldsymbol{q}_i)$, $\varepsilon_f \geqslant 0$, corresponding to the wave-packet bin that contains the electron momentum $\boldsymbol{\kappa}$,

$$T_{fi}^{\mathrm{DI}}(\boldsymbol{\kappa}, \boldsymbol{q}_f, \boldsymbol{q}_i) = \frac{1}{(2\pi)^{3/2}}\sum_{\ell m}\langle\psi_{\boldsymbol{\kappa}}^{\mathrm{T}}|\psi_f^{\mathrm{T}}\rangle T_{fi}^{\mathrm{DS}}(\boldsymbol{q}_f, \boldsymbol{q}_i). \tag{7}$$

Here $\langle\psi_{\boldsymbol{\kappa}}^{\mathrm{T}}|\psi_f^{\mathrm{T}}\rangle$ is the overlap between the true continuum wave solution of the Schrödinger equation for an electron in the presence of the residual target ion $\psi_{\boldsymbol{\kappa}}^{\mathrm{T}}$ and the wave-packet pseudostate ψ_f^{T}. The summation over ℓ and m appears due to the different wave-packet pseudostates within the same momentum bin that have differing angular momentum and magnetic quantum numbers having the same energy. The second term corresponds to electron capture into the continuum (ECC) of the projectile and is given by

$$T_{fi}^{\mathrm{ECC}}(\boldsymbol{\varkappa}, \boldsymbol{q}_f, \boldsymbol{q}_i) = \frac{1}{(2\pi)^{3/2}}\sum_{\ell m}\langle\psi_{\boldsymbol{\varkappa}}^{\mathrm{P}}|\psi_f^{\mathrm{P}}\rangle T_{fi}^{\mathrm{EC}}(\boldsymbol{q}_f, \boldsymbol{q}_i), \tag{8}$$

where $\boldsymbol{\varkappa}$ is the electron momentum in the projectile-centred frame, and $\langle\psi_{\boldsymbol{\varkappa}}^{\mathrm{P}}|\psi_f^{\mathrm{P}}\rangle$ is the overlap between the pure Coulomb wave, $\psi_{\boldsymbol{\varkappa}}^{\mathrm{P}}$, and wave-packet pseudostate ψ_f^{P}. The fully differential cross section for ionization is given by

$$\begin{aligned} \frac{\mathrm{d}^3\sigma_n}{\mathrm{d}E_\mathrm{e}\mathrm{d}\Omega_\mathrm{e}\mathrm{d}\Omega_f} = \frac{\mu_\mathrm{T}^2}{(2\pi)^2}\frac{q_f\kappa}{q_i}\big(&\big|T_{fi}^{\mathrm{DI}}(\boldsymbol{\kappa}, \boldsymbol{q}_f, \boldsymbol{q}_i)\big|^2 \\ &+ \big|T_{fi}^{\mathrm{ECC}}(\boldsymbol{\kappa} - \boldsymbol{v}, \boldsymbol{q}_f, \boldsymbol{q}_i)\big|^2\big). \end{aligned} \tag{9}$$

The DI and ECC amplitudes are calculated in the target-centered and projectile-centered frames, respectively. They must be brought into a common frame before combining to calculate the FDCS for ionization. We choose the laboratory frame to allow for comparison with experimental results. Hence, the ECC component is transformed into the laboratory frame.

The momentum-space scattering amplitudes are given by the Fourier-Bessel transform of the asymptotic values of the expansion coefficients in Eq. (2) obtained from solving Eq. (3). After performing the integration over the parallel component of the momentum transfer analytically, all that remains is to evaluate the integral over the perpendicular momentum transfer. Therefore, the direct-scattering amplitudes calculated according to

$$T_{fi}^{\mathrm{DS}}(\boldsymbol{q}_f, \boldsymbol{q}_i) = 2\pi i v \mathrm{e}^{im\phi_f}\int_0^\infty \mathrm{d}\, b\, b[\tilde{F}_f(+\infty, b) - \delta_{fi}]J_m(q_\perp b), \tag{10}$$

where $\boldsymbol{q}_\perp$ is the perpendicular component of the momentum transfer $\boldsymbol{q} = \boldsymbol{q}_i - \boldsymbol{q}_f$, $\tilde{F}_f(t, b) = \mathrm{e}^{im\phi_b}F_f(t, \boldsymbol{b})$, ϕ_f is the azimuthal angle of $\boldsymbol{q}_f$, m is the magnetic quantum number of the final state, and J_m is the Bessel function of the mth order. Here, we assume that the magnetic quantum number of the initial state is $m_i = 0$.

Similarly, the electron capture amplitudes are given by

$$T_{fi}^{\mathrm{EC}}(\boldsymbol{q}_f, \boldsymbol{q}_i) = 2\pi i v \mathrm{e}^{im\phi_f}\int_0^\infty \mathrm{d}\, b\, b\tilde{G}_f(+\infty, b)J_m(q_\perp b), \tag{11}$$

where $\tilde{G}_f(t, b) = \mathrm{e}^{im\phi_b}G_f(t, \boldsymbol{b})$.

The coupled equations formed by substituting Eq. (2) into Eq. (1) are solved at 64 impact-parameter points from $b_{\min} = 0$ to $b_{\max} = 40$ a.u. Evaluation of the integrals

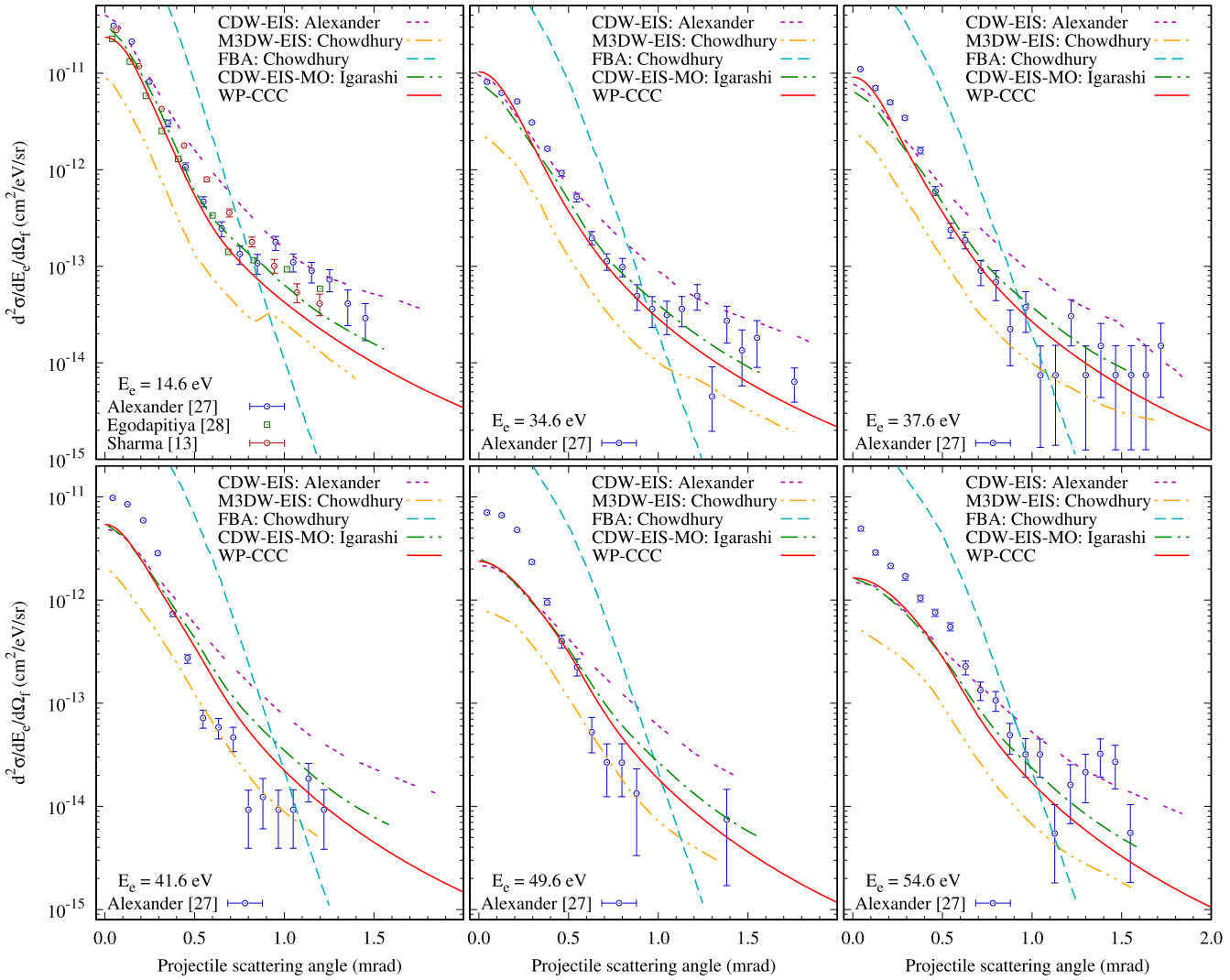

FIG. 1. Doubly differential cross section of ionization for 75-keV proton collisions with H_2 as a function of the scattering angle of the projectile at various ejection energies. Results are presented in the laboratory frame. Experimental data are by Alexander *et al.* [27], Egodapitiya *et al.* [28], and Sharma *et al.* [13]. Theoretical results: The present WP-CCC approach, the continuum-distorted-wave eikonal-initial-state method by Alexander *et al.* [27], the molecular three-body distorted-wave eikonal-initial-state method and first-order Born approximation by Chowdhury *et al.* [29], and continuum-distorted-wave eikonal-initial-state molecular-orbital method by Igarashi and Gulyás [32].

in Eqs. (10) and (11) is then achieved using the fast Hankel transform algorithm of Anderson [45]. This method is very accurate and capable of handling large values of perpendicular momentum-transfer without the need to know the amplitudes at a very large number of impact-parameter points.

III. RESULTS

In this section we present the results of our calculations for the doubly differential ionization cross section as a function of the projectile scattering angle and energy of the ejected electron, and as a function of the projectile scattering angle and emission angle of the ejected electron. We find that a basis including $10 - \ell$ bound states for each orbital angular momentum up to $\ell_{\max} = 7$ was sufficient to obtain convergence in the results. We used 25 discrete continuum bins up to a maximum electron momentum of 6 a.u. Increasing this cutoff made no appreciable difference to the final results. The total number of states used in the expansion in Eq. (2) was therefore 3864. The z grid contained 2000 points from -400 to $+400$ a.u., relative to the target nucleus. The DDCS was checked by integrating twice and comparing the result against the independently calculated total ionization cross section (TICS) from the expansion coefficients to ensure they were the same as those reported in Ref. [38].

Figure 1 shows our calculated DDCS for ionization as a function of the scattering angle of the projectile at selected electron-emission energies. Specifically, results are presented for electron energies of 14.6, 34.6, 37.6, 41.6, 49.6, and 54.6 eV, where experimental data are available. The projectile energy is 75 keV, which corresponds to a speed of $v_i = 1.733$ a.u. At the matching speed, the emitted electron would have an energy of 40.8 eV.

In the top left panel we present results for an electron energy of 14.6 eV. The three sets of experimental data

available at this emission energy agree well with one another for scattering angles less than 0.5 mrad. However, at larger scattering angles the data of Alexander *et al.* [27] and Egodapitiya *et al.* [28] suggest the presence of some structure around 1.0 mrad, whereas the measurements reported by Sharma *et al.* [13] do not. Note that Sharma *et al.* [13] claims their data for angles greater than 0.8 mrad is more accurate than the previously reported measurements due to improvements in the removal of background signals. The CDW-EIS calculations by Alexander *et al.* [27] agree with the experimental data in the forward direction but from 0.4–0.9 mrad they overestimate the data from Alexander *et al.* [27] and Egodapitiya *et al.* [28]. Above this the CDW-EIS calculations agree with the magnitude of data recorded by Alexander *et al.* [27], but do not reproduce the shape. As the scattering angle increases the CDW-EIS results fall off more slowly than all other results. The M3DW-EIS calculations by Chowdhury *et al.* [29] generally reproduce the shape of the experimental data, including the structure reported by Alexander *et al.* [27] around 1.0 mrad. However, they are consistently too small across all scattering angles. The FBA results of Chowdhury *et al.* [29] demonstrate significant disagreement with all experimental and other theoretical results. In the forward direction the FBA vastly overestimates the DDCS, then falls off steeply and underestimates the other results at large scattering angles. In Fig. 1 we include the CDW-EIS-MO results by Igarashi and Gulyás [32]. The CDW-EIS-MO calculations more closely follow the experimental data than the other available theoretical results. In particular, they agree very well with the measurements by Alexander *et al.* [27] at scattering angles less than 0.9 mrad, then continue to fall off smoothly, similarly to the data of Sharma *et al.* [13]. The present WP-CCC results agree very well with the experimental data of Alexander *et al.* [27] and Sharma *et al.* [13] in the forward direction, then from 0.4–0.9 mrad they continue to closely follow the data of Alexander *et al.* [27], slightly underestimating the measurements by Sharma *et al.* [13]. Our calculations show no evidence of any structure at large scattering angles, instead falling off smoothly in agreement with the data by Sharma *et al.* [13] above 1.0 mrad.

The remaining panels in Fig. 1 show the DDCS results at the other emission energies where Alexander *et al.* [27] reported experimental data. At 34.6 eV, the situation is very similar to that at 14.6 eV. The WP-CCC results agree well with the experiment up to a scattering angle of 1.2 mrad. However, thereafter, the structure suggested by Alexander *et al.* [27] is not replicated by our calculations. In the forward direction our results are very similar to the CDW-EIS and CDW-EIS-MO calculations, but above 0.5 mrad the WP-CCC results decrease like the CDW-EIS-MO results in agreement with the experimental data whereas the CDW-EIS calculation begins to fall off less steeply. The M3DW-EIS result is again in qualitative agreement with the experiment, but consistently underestimates the magnitude.

At 37.6, 41.6, and 49.6 eV, the structure suggested by the measurements of Alexander *et al.* [27] is less pronounced or absent. As a result, improved agreement between the WP-CCC results and the experiment is observed at large scattering angles. However, like in all other calculations, at small scattering angles significant discrepancies are observed when more energetic electrons are ejected. The CDW-EIS-MO ones also agree better with experiment. However, in the forward direction all available theoretical results underestimate the experimental measurements. The experimental data of Alexander *et al.* [27] suggests a narrowing of the forward peak at emission energies near the 40.8 eV where the speed of the electron matches that of the projectile. However, our results agree with the CDW-EIS-MO prediction that the DDCS should continue to steadily decrease in magnitude, without significantly changing shape. At an emission energy of 54.6 eV the experimentally measured DDCS falls off at a similar rate to that recorded at 14.6 and 34.6 eV. The theoretical results are in better agreement with the experiment at this energy than at 37.6, 41.6, and 49.6 eV. However, the experimental data of Alexander *et al.* [27] again suggest some form of structure at large scattering angles which could not be resolved in the data at 49.6 eV. None of the available theoretical results support this observation at any of the emission energies considered. Across all emission energies considered the WP-CCC calculations agree well with the CDW-EIS method in the forward direction, however, they underestimate it at large scattering angles. Our results are consistently very close to those from Igarashi and Gulyás [32] and always overestimate the M3DW-EIS calculations by Chowdhury *et al.* [29].

To summarize, we find that the WP-CCC results demonstrate very good agreement with the CDW-EIS-MO calculations by Igarashi and Gulyás [32] and both methods more consistently reproduce the experimental data than the other available theoretical approaches. The CDW-EIS calculations by Alexander *et al.* [27] show a similar level of agreement in the forward direction, but consistently overestimate the experiment and CDW-EIS-MO and WP-CCC results as the scattering angle increases. The M3DW-EIS calculations consistently underestimate the experimental data and other theoretical methods, although the shape is very similar to the CDW-EIS-MO and WP-CCC results qualitatively, except for the small peak present in the M3DW-EIS results for 14.6 eV electrons. With the exception of the not yet fully understood structure in the experimental data of Alexander *et al.* [27] and Egodapitiya *et al.* [28] at large scattering angles, the WP-CCC calculations demonstrate very good agreement with experiment at 14.6, 34.6, and 37.6 eV. At higher emission energies agreement is less satisfactory, in particular, when the electron's speed is close to the projectile's. At both 41.6 and 49.6 eV the WP-CCC calculations fall off less steeply than the experimental data and underestimate the measured DDCS in the forward direction. Calculation of the DDCS for ionization is easiest at the smallest scattering angles. Moreover, we find very close agreement between the CDW-EIS, CDW-EIS-MO, and WP-CCC results at all considered electron energies when the projectile is scattered into the forward direction. Therefore, the discrepancy between theory and experiment for small scattering angles observed in the lower three panels in Fig. 1 is somewhat puzzling.

The experimental data by Sharma *et al.* [13] do not support the structure observed at large scattering angles by the other two experiments. However, improved data for large scattering angles is not available for other emission energies. Interestingly, the TICS obtained by integrating our DDCS was consistent with our earlier result obtained directly. We recall

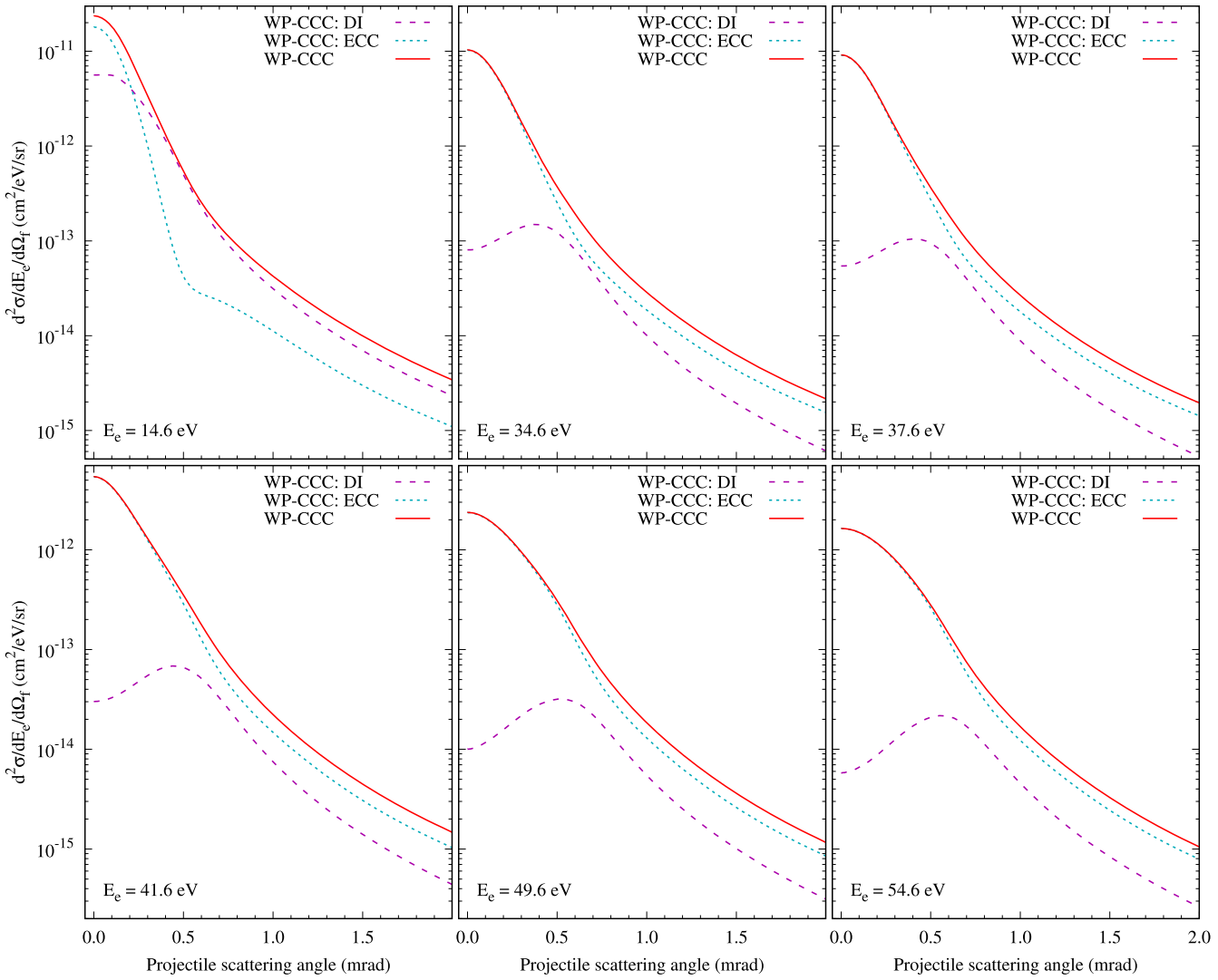

FIG. 2. DI and ECC components of the total WP-CCC doubly differential cross section for ionisation shown in Fig. 1.

that at 75 keV it was found to slightly overestimate experiment [38]. Consequently, we would expect our DDCS for ionisation to generally be slightly larger than experiment, but in fact we see the opposite.

A possible reason for the observed discrepancy between calculation and experiment for large electron energies could be the omission of electron-correlation effects in the theoretical models. However, this appears to be a reasonable approximation for calculating integrated [38] and singly differential [39] cross sections at intermediate projectile energies. Furthermore, the present approach gives excellent agreement with the experimental data for the DDCS as a function of the energy and angle of the ejected electrons [25,26]. Nevertheless, the DDCS in the electron energy and projectile angle could be more sensitive to this approximation. Another possibility could be that the present theoretical cross section represents a slightly different quantity to the measured data. Calculations are performed at exact angles and energies. In contrast, the apparatus have finite resolution and therefore each data point represents an integration over the angular and energy resolutions of the detector. This potentially could influence the cross sections. However, the experimental data of Refs. [13,27,28] were not deconvolved because the effect was found to be small. In principle, the experimental resolution may mostly affect the small angles. As seen in the lower three panels of Fig. 1, when more energetic electrons are emitted, the disagreement in the forward direction is as large as 70%. It is difficult to expect that electron-correlation effects can change the present results by that much. We should also mention that the WP-CCC approach to doubly differential ionization in $p+$He collisions with and without electron-correlations effects [46,47] gave practically the same result in all domains including the forward-scattering angle. In any case, the reason for the discrepancy remains to be understood and warrants further investigation.

In Fig. 2 we show the same WP-CCC results as in Fig. 1, but this time together with the DI and ECC components. In our approach to differential ionization, the total cross section is given by the sum of these contributions. The ability to separate these two contributions can provide insight into the mechanisms responsible for ionisation in different kinematic regions. Although we emphasise that the DI and ECC components do not individually represent physical cross sections. The total DDCS is separated into these two distinct parts as

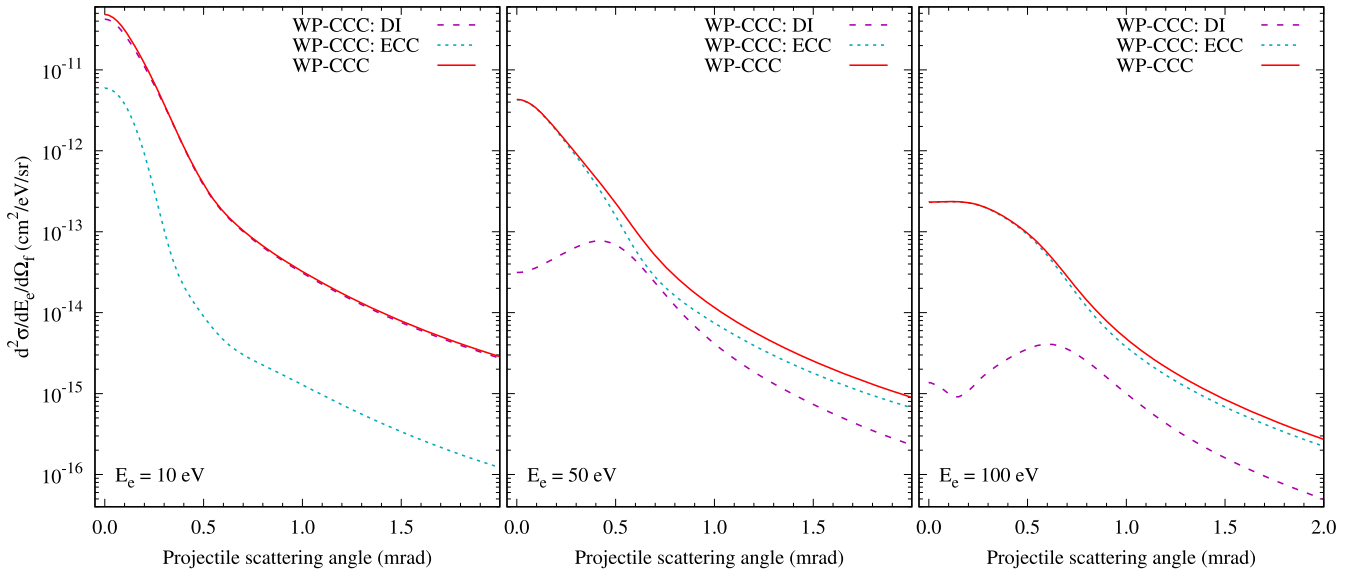

FIG. 3. Doubly differential cross section for ionization in $p + H_2$ collisions for a projectile energy of 100 keV. The DI and ECC components of the total WP-CCC result are also shown.

a result of the two-center formalism. At all emission energies considered, except the smallest, we see that the forward scattering DDCS is dominated by the ECC mechanism. As the emission energy increases this becomes more pronounced. Physically this can be explained by the emitted electron being pulled along by the attractive charge of the projectile. Higher-energy electrons are traveling faster, making it more likely for them to be closer to the projectile nucleus than the target nucleus if they are emitted into the forward cone. At larger scattering angles DI and ECC are generally of similar magnitude, with DI dominating at low-energy electrons and gradually becoming less significant as the energy increases. However, at all considered emission energies both DI and ECC play a significant role in the total DDCS for ionisation.

In Figs. 3 and 4 we present the DDCS for ionization differential in the projectile scattering angle and electron energy at incident energies of 100 and 200 keV, respectively. We show the DDCS and DI and ECC components for protons incident on H_2. The electron energy that corresponds to the matching speed is 54.4 and 114.3 eV for 100 and 200 keV projectiles, respectively. There are no experimental data available at these projectile energies. As one can see, DI and ECC both make significant contributions to the total DDCS at all three emission energies. For 10 eV electrons, the DI component is dominant across all scattering angles, whereas at 50 eV ECC is two orders of magnitude larger in the forward direction. At 0.5 mrad both components are comparable, and DI becomes the larger contributor at higher scattering angles. For 100 eV emission ECC is the dominant mechanism from 0 to 2.0 mrad.

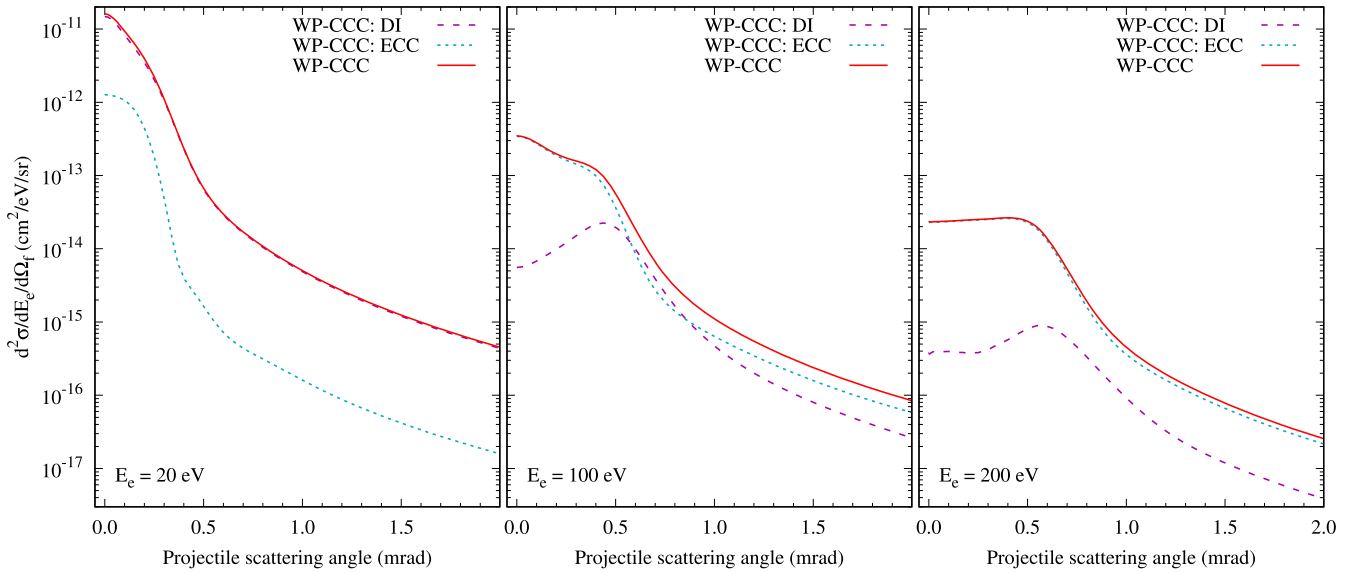

FIG. 4. Doubly differential cross section for ionization in $+H_2$ collisions for a projectile energy of 200 keV. The DI and ECC components of the total WP-CCC result are also shown.

Since this energy corresponds to an electron speed much larger than the projectile speed and electron emission near forward angles is most likely, this suggests that the majority of high-energy electrons leave the scattering system ahead of the projectile.

At an incident energy of 200 keV, we see that the DI component is less significant in the forward direction. For 100 eV electrons the results show a small shoulder around 0.5 mrad. For emission of 200 eV electrons the DDCS is almost constant from 0 to 0.5 mrad. This is similar to the behavior observed for ejection of 100 eV electrons by 100 keV proton collisions in Fig. 3. The origin of this behavior is unknown. However, it is reminiscent of the secondary-peak observed in angular differential cross sections for electron capture by positively charged ions at projectile energies in the MeV region. The secondary peak in electron capture DCS is attributed to the Thomas double-scattering mechanism [48]. According to this classical explanation, the projectile scatters the target electron by 60°, transferring energy and increasing the electron speed to approximately that of the projectile. Then, the electron elastically scatters from the residual target ion, altering its trajectory by 60° again such that it leaves the scattering system in approximately the same direction as the projectile. The momentum transfer required for this corresponds to a projectile scattering angle of 0.47 mrad. Therefore, the DCS for electron capture is increased at this angle. The structure observed in the present DDCS for ionization occurs very close to the Thomas angle and is primarily caused by the ECC component. Perhaps it is possible that the Thomas mechanism is causing a secondary peak in the DDCS for ionization by increasing the probability of ECC near 0.47 mrad. However, the projectile energies considered herein are significantly smaller than those typically associated with the Thomas mechanism. This feature is only observed in the DDCS for ionization for the emission of electrons with large energies and is not significant enough to have an effect on the SDCS for ionization [39]. It should be noted, however, that the rather pronounced peak structure in the DI channel is not due to the Thomas process. Rather, it can be explained as a simple effect of the kinematic conservation laws in a binary process.

To analyze the rate of fall-off of the DDCS for ionization, we calculated the average scattering angle as a function of electron energy for the results shown in Fig. 2. The average scattering angle of the projectile is given by the normalized expectation value

$$\langle\theta_f\rangle = \frac{\int \frac{\mathrm{d}^2\sigma}{\mathrm{d}E_e\mathrm{d}\Omega_f}\theta_f \mathrm{d}\Omega_f}{\int \frac{\mathrm{d}^2\sigma}{\mathrm{d}E_e\mathrm{d}\Omega_f}\mathrm{d}\Omega_f}. \tag{12}$$

We present results for H_2 and also He and H targets in Fig. 5, along with experimental data by Schulz *et al.* [49] and Silvus *et al.* [50]. Calculations of the DDCS for ionization differential in the scattering angle of the projectile and energy of the electron are presented for the H and He targets in Refs. [33,47], respectively. The horizontal axis shows the speed of the ejected electron in units of the projectile speed. For atomic hydrogen we use the exact eigenstates and true Coulomb wave solution to construct the basis states. For the helium target we use the effective one-electron approach detailed in Refs. [34,35]. In the top panel the maximum scattering angle entering the integrals in Eq. (12) is sufficiently large that the value of the average scattering angle is convergent. However, experimental data for the DDCS are only available for a limited range of scattering angles. Therefore, in the lower panel of Fig. 5 we show our results for the average scattering angle calculated with θ_f truncated at the largest scattering angle for which experimental data are available for each system.

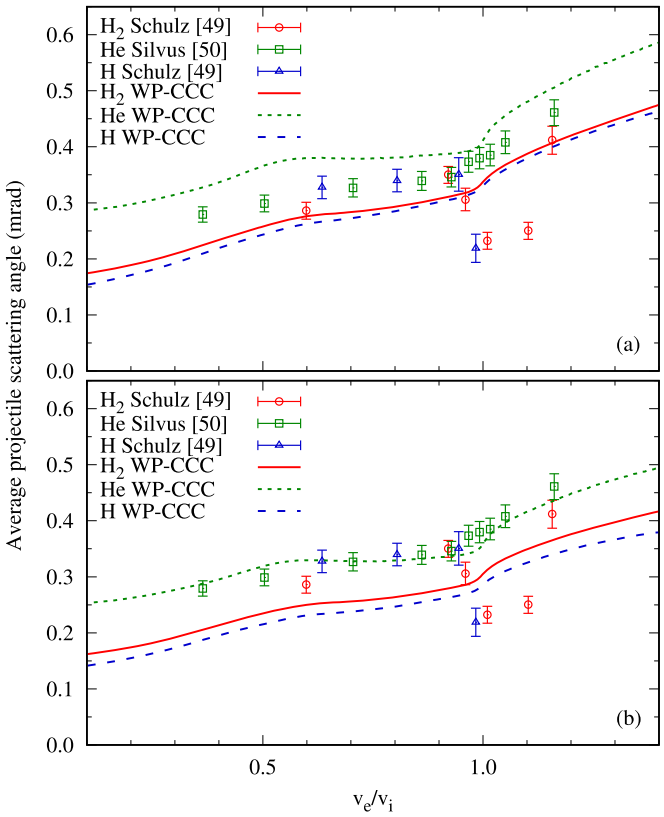

FIG. 5. Average projectile scattering angle for ionizing collisions of 75-keV protons with H_2, He, and H as a function of the speed of the electron in units of the projectile speed. Panel (a) shows the converged WP-CCC results. Panel (b) shows the results obtained when the maximum angle used in calculation of the average scattering angle for the WP-CCC results is restricted to the largest angle recorded in each set of experimental data. Experimental data are by Schulz *et al.* [49] and Silvus *et al.* [50].

First analyzing the convergent calculations in the upper panel of Fig. 5, we find that results for atomic hydrogen yield similar DDCS for ionization as for molecular hydrogen. Our results for the DDCS for the H_2 target are consistently larger than for He in the forward direction. In this region the ECC mechanism dominates. This suggests that electron capture into the continuum of the projectile has a stronger effect for the H_2 target. For larger scattering angles, the DI component for the He results is larger than for the H_2 calculations. Since DI is comparable to ECC at large angles, this results in an overall larger total DDCS for helium at large scattering angles. These differences in the DDCS can be explained by the change in ionization energy between the hydrogen molecule and helium atom. Significantly more energy is required to ionize He, hence the probability (and therefore the cross section)

for ionization is expected to be smaller compared to that for H_2. Upon integration of our results for the DDCS for ionization at 75 keV, we obtain a TICS for the H_2 and He targets of 2.29×10^{-16} cm^2 and 0.98×10^{-16} cm^2, respectively.

The average scattering angle for our helium calculations shown in the upper panel of Fig. 5 is consistently larger than for molecular hydrogen. For H_2 and H, the calculated average scattering angle increases steadily up until the matching speed, in agreement with the experimental data in this region. However, near $v_e/v_i = 1$ the experimentally measured average scattering angle drops significantly whereas our results continue to increase. This dip in the average scattering angle corresponds to the narrowing of the DDCS observed at energies near the matching speed in Fig. 1. Schulz *et al.* [49] suggested that this behavior may be the result of the attractive Coulomb interaction between the projectile ion and ionized electron causing a mutual focusing effect. In our method all interactions between the target residual ion, projectile ion, and active electron are explicitly accounted for in the total Hamiltonian of the scattering system. However, our results show no evidence of a decrease in average scattering angle near the matching speed for either atomic or molecular hydrogen targets. Interestingly, our calculations for the helium target consistently overestimate the experimental data which is of a similar magnitude to the data for H_2 and H when $v_e/v_i < 1$. At the matching speed the WP-CCC results begin to increase more steeply in qualitative agreement with the experimental data for helium. It has been suggested that the ionization energy of the target thus has an effect on the strength of the interaction between the projectile and electron in the exit channel [50] and that this may be responsible for the difference in the experimentally measured average scattering angle near the matching speed. Atomic and molecular hydrogen have relatively similar ionization energies of 0.5 and 0.598 a.u., respectively, whereas the ionisation energy of helium is 0.904 a.u. However, our results suggest this is not the case as the average scattering angle shows no evidence of a decrease around the matching speed.

Restricting θ_f to the range where the experimental data was recorded significantly affects the results as shown in the lower panel in Fig. 5. While the shape of our calculations is mostly unchanged, the magnitude is decreased for all three scattering systems. Consequently, agreement between our calculations and the experimental data for He is significantly improved. However, discrepancies between the calculations and experimental data for H and H_2 remain.

Finally, for completeness, in Fig. 6 we present the DDCS for ionization of H_2 by proton impact as a function of the scattering angle of the projectile and emission angle of the ejected electron. The azimuthal angle of the electron is measured relative to the scattering plane, i.e., $\phi_f = 0$. Since the interaction between the particles is symmetric relative to the scattering plane, we include angles only for one hemisphere of the collision geometry. To the best of our knowledge there are no experimental measurements or calculations of this type of DDCS for $p + H_2$ available in the literature. For comparison we present FBA calculations as well. Each row in Fig. 6 shows our results for electrons emitted at a fixed polar angle θ_e with varying azimuthal angle, ϕ_e. Each column represents emission into a fixed azimuthal angle for different polar angles. For small scattering angles the FBA results are larger or comparable to the WP-CCC calculations across all considered collision geometries. Conversely, at the larger scattering angles the FBA results fall off much more rapidly. The overall magnitude of the WP-CCC calculations decreases with increasing θ_e for all considered azimuthal angles, suggesting emission in the forward direction is more likely. However, for a fixed polar angle, different values of ϕ_e have less of an effect on the magnitude of the cross section. Instead, we see that the shape of the DDCS is influenced by the azimuthal angle.

IV. CONCLUSION

In this work we applied the two-center wave-packet convergent close-coupling approach to calculate the two types of the doubly differential cross section for ionization that are functions of the scattering angle of the projectile for proton collisions with molecular hydrogen. For the first type that depends also on the energy of the ejected electron, we found good agreement with the most recent experimental results by Sharma *et al.* [13] at the smallest emission energy where data are available. The structure observed at large scattering angles in the data of Alexander *et al.* [27] and Egodapitiya *et al.* [28] is not reproduced by our results. Furthermore, we find that the general agreement with experiment is best for emission energies smaller than the energy corresponding to the emitted electron having the same speed as the projectile. For emission energies resulting in electron emission with comparable or higher speed than the projectile's the WP-CCC results predict a significantly smaller forward peak and fall off more slowly than the experimental data. A similar behavior is seen in other available calculations. In particular, our calculations are very close to the CDW-EIS-MO results of Igarashi and Gulyás [32] at all considered emission energies. However, the WP-CCC method incorporates strong coupling effects between all significant reaction channels and coupling to the ionisation continuum of the electron, neither of which are considered in previously available calculations.

Our results, as well as some distorted wave calculations, did not reproduce the structure observed in Refs. [27,28] at large scattering angles. Furthermore, in the data of Ref. [13] this structure was only found in the coherent to incoherent DDCS ratios, but not in the absolute DDCS. Therefore, the role of two-center effects in the DDCS is still an open question.

The WP-CCC method is capable of explicitly differentiating between the separate contributions of direct ionization and electron capture into the continuum of the projectile to the full DDCS result. It was found that DI is most significant for scattering in the forward direction for electrons emitted with small energies, while for high-energy electrons ECC dominates in the forward direction but both components are significant at large scattering angles. For electrons with energies near or above the matching speed, ECC is found to be the dominant mechanism for ionization for scattering in the forward direction, as expected. When an electron is near the projectile or on the other side of the projectile from the target it will be much more likely for it to reside in the continuum of the projectile atom. Our present results are the first available

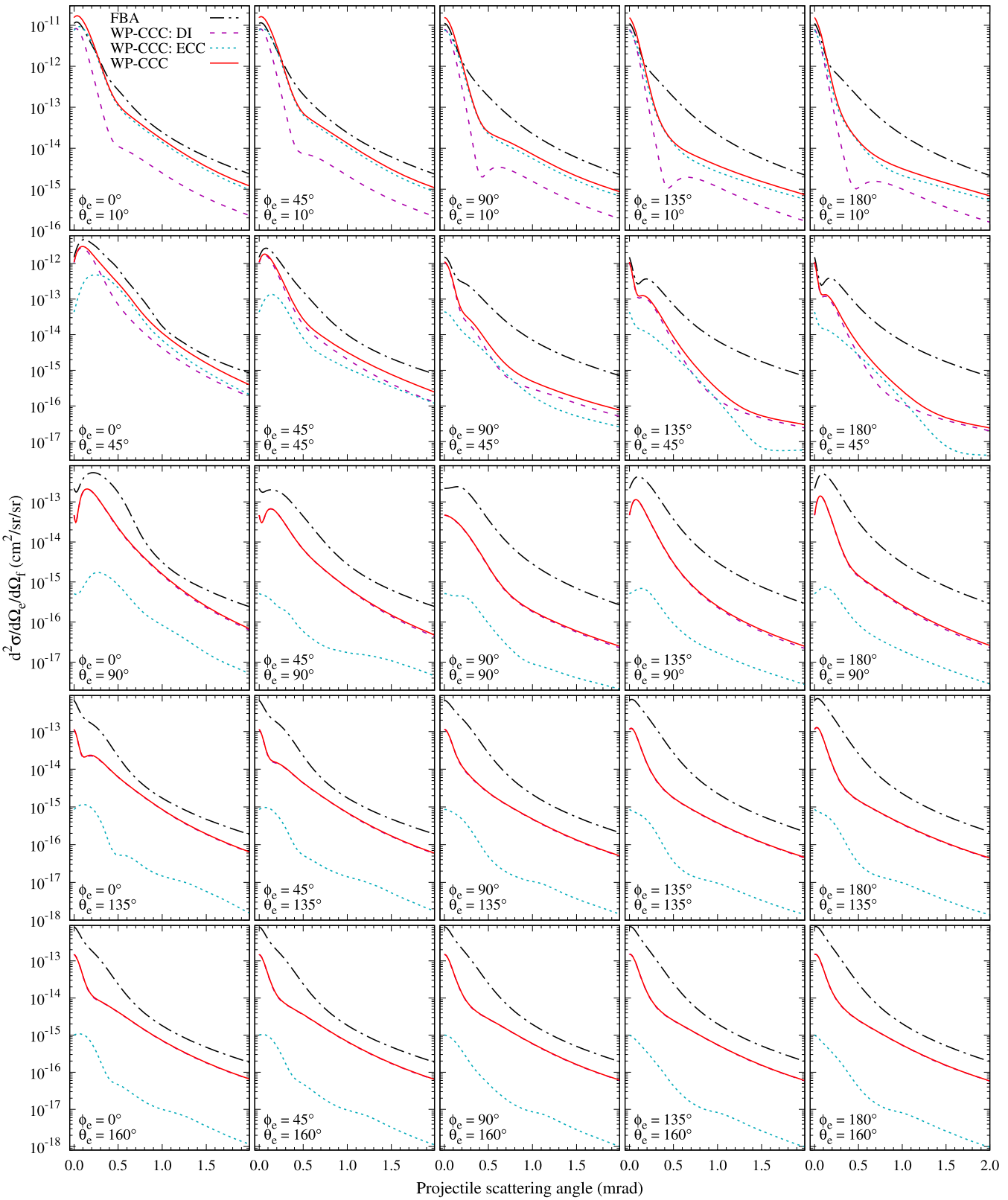

FIG. 6. Doubly differential cross section for ionization for 75-keV proton collisions with H_2 as a function of the scattering angle of the projectile at different emission angles. Results are presented in the laboratory frame. The present DI and ECC components are also shown. The key in the upper-left panel applies to all panels.

calculations to explicitly identify the contributions of these mechanisms in the DDCS for ionization in $p + H_2$ collisions.

Results for the DDCS for ionisation as a function of projectile scattering angle and electron energy at 100 and 200 keV are also presented. When the electron energy is comparable to or larger than the matching speed we see evidence of a secondary peak near the classical Thomas angle. There are no other calculations or experimental data available for comparison. Furthermore, the currently considered projectile energies are lower than those typically associated with the Thomas double-scattering mechanism. However, the present results could be explained as an enhanced ECC probability resulting from a similar double-scattering mechanism.

We also present calculations of the average scattering angle ionization as a function of the speed of the emitted electron. Results for H, H_2, and He are compared with experiment. We find that the helium cross sections have a consistently shallower fall-off compared to both atomic and molecular hydrogen, favoring larger scattering angles. The present results for the average scattering angle were found to qualitatively agree for He, although the magnitude of the experimental data are overestimated. For H and H_2, the average scattering angle agrees well with experiment, except near the matching speed where a significant decrease in the experimental data is not reproduced by our results. Restricting the maximum angle to the largest experimentally measured angle was found to significantly improve the quantitative agreement between the WP-CCC calculations and experiment, but only for He. Overall, the present results do not reproduce the minima found in the measured average scattering angles as a function of v_e/v_i in the case of H and H_2.

In conclusion, we calculated two types of doubly differential cross section for ionization in $p + H_2$ collisions. The first as a function of the projectile scattering angle and emitted electron energy and the second as a function of the projectile scattering angle and emission angle of the ejected electron. Agreement with experimental data is generally good, although differences exist for some emission energies. We also present results for the average scattering angle for ionising collisions as a function of the relative speed of the emitted electron. With this we have now calculated all types of singly and doubly differential cross sections for single-ionisation in $p + H_2$ collisions using the two-center WP-CCC method [25,39]. Previously we also investigated total cross sections [38] for direct scattering, electron capture, and ionization as well as angular differential cross sections for binary processes. Agreement with available experimental data is generally very good, although some differences were noted in the DDCS studied herein. Having verified the accuracy and reliability of the approach when applied to integrated, singly differential, and doubly differential cross sections, we will next turn our attention to the fully differential cross section for ionization. This is the most detailed type of single-electron ionization cross section in this scattering system and presents a significant theoretical challenge. Currently available calculations do not agree with one another and agreement with experiment is inconsistent [14]. Using the WP-CCC method we will next calculate the FDCS with the aim of reconciling this discrepancy between theory and state-of-the-art experiment. The explicit inclusion of projectile-centered pseudostates allows us to accurately model the ECC mechanism, and the close-coupling formalism incorporates the interactions between all of the many significant reaction channels. It is currently unknown if the discrepancies are the result of interference between first and higher-order scattering amplitudes, inadequate description of the ECC mechanism, two-center interference, or another yet-to-be-discovered reason [13]. The present WP-CCC method should be capable of assessing the impact of the first two processes. We also plan to develop a more detailed target description that would allow us to investigate the influence of two-center interference on the cross sections within the WP-CCC framework.

ACKNOWLEDGMENTS

This work was supported by the Australian Research Council. We also acknowledge the resources and services of the Pawsey Supercomputer Centre and the National Computing Infrastructure. C.T.P. acknowledges support through an Australian Government Research Training Program Scholarship. K.H.S. acknowledges the contribution of an Australian Government Research Training Program Scholarship, and the support of the Forrest Research Foundation. M.S. is grateful for the support from the National Science Foundation under Grant No. PHY-2011307.

[1] *Ion-Atom Collisions: The Few-Body Problem in Dynamic Systems*, edited by M. Schulz (De Gruyter, Berlin, 2019).
[2] *State-of-the-Art Reviews on Energetic Ion-Atom and Ion-Molecule Collisions*, edited by Dž. Belkić, I. Bray, and A. Kadyrov (World Scientific, Singapore, 2019).
[3] E. Speth, Rep. Prog. Phys. **52**, 57 (1989).
[4] A. Kirk, Contemp. Phys. **57**, 1 (2016).
[5] O. Marchuk, Phys. Scr. **89**, 114010 (2014).
[6] N. Schwadron and T. Cravens, Astrophys. J. **544**, 558 (2000).
[7] R. Von Steiger, N. Schwadron, L. Fisk, J. Geiss, G. Gloeckler, S. Hefti, B. Wilken, R. Wimmer-Schweingruber, and T. Zurbuchen, J. Geophys. Res. **105**, 27217 (2000).
[8] Dž. Belkić, J. Math. Chem. **47**, 1366 (2010).
[9] R. P. Levy, E. A. Blakely, W. T. Chu, G. B. Coutrakon, E. B. Hug, G. Kraft, and H. Tsujii, in *AIP Conf. Proc.*, Vol. 1099 (American Institute of Physics, Melville, NY, 2009), pp. 410–425.
[10] P. de Vera, I. Abril, and R. Garcia-Molina, Radiat. Res. **190**, 282 (2018).
[11] R. Dörner, V. Mergel, O. Jagutzki, L. Spielberger, J. Ullrich, R. Moshammer, and H. Schmidt-Böcking, Phys. Rep. **330**, 95 (2000).
[12] J. Ullrich, R. Moshammer, A. Dorn, R. Dörner, L. P. H. Schmidt, and H. Schmidt-Böcking, Rep. Prog. Phys. **66**, 1463 (2003).

[13] S. Sharma, T. P. Arthanayaka, A. Hasan, B. R. Lamichhane, J. Remolina, A. Smith, and M. Schulz, Phys. Rev. A **89**, 052703 (2014).
[14] M. Dhital, S. Bastola, A. Silvus, B. R. Lamichhane, E. Ali, M. F. Ciappina, R. Lomsadze, A. Hasan, D. H. Madison, and M. Schulz, Phys. Rev. A **100**, 032707 (2019).
[15] S. Bastola, M. Dhital, B. Lamichhane, A. Silvus, R. Lomsadze, J. Davis, A. Hasan, A. Igarashi, and M. Schulz, Phys. Rev. A **105**, 032805 (2022).
[16] M. Dhital, S. Bastola, A. Silvus, A. Hasan, B. R. Lamichhane, E. Ali, M. F. Ciappina, R. A. Lomsadze, D. Cikota, B. Boggs, D. H. Madison, and M. Schulz, Phys. Rev. A **99**, 062710 (2019).
[17] B. R. Lamichhane, T. Arthanayaka, J. Remolina, A. Hasan, M. F. Ciappina, F. Navarrete, R. O. Barrachina, R. A. Lomsadze, and M. Schulz, Phys. Rev. Lett. **119**, 083402 (2017).
[18] S. Zou, L. Pichl, M. Kimura, and T. Kato, Phys. Rev. A **66**, 042707 (2002).
[19] A. Igarashi and C. D. Lin, Phys. Rev. Lett. **83**, 4041 (1999).
[20] Dž. Belkić, *Quantum Theory of High-Energy Ion-Atom Collisions* (CRC Press, Boca Raton, FL, 2008).
[21] R. E. Olson and A. Salop, Phys. Rev. A **16**, 531 (1977).
[22] C. Illescas and A. Riera, Phys. Rev. A **60**, 4546 (1999).
[23] M. Schulz, T. Vajnai, A. D. Gaus, W. Htwe, D. H. Madison, and R. E. Olson, Phys. Rev. A **54**, 2951 (1996).
[24] D. Schultz, H. Gharibnejad, T. E. Cravens, and S. Houston, At. Data Nucl. Data Tables **132**, 101307 (2020).
[25] C. T. Plowman, I. B. Abdurakhmanov, I. Bray, and A. S. Kadyrov, Phys. Rev. A **107**, 032824 (2023).
[26] C. T. Plowman, K. H. Spicer, and A. S. Kadyrov, Atoms **11**, 112 (2023).
[27] J. S. Alexander, A. C. Laforge, A. Hasan, Z. S. Machavariani, M. F. Ciappina, R. D. Rivarola, D. H. Madison, and M. Schulz, Phys. Rev. A **78**, 060701(R) (2008).
[28] K. N. Egodapitiya, S. Sharma, A. Hasan, A. C. Laforge, D. H. Madison, R. Moshammer, and M. Schulz, Phys. Rev. Lett. **106**, 153202 (2011).
[29] U. Chowdhury, M. Schulz, and D. H. Madison, Phys. Rev. A **83**, 032712 (2011).
[30] J. Gao, J. L. Peacher, and D. H. Madison, J. Chem. Phys. **123**, 204302 (2005).
[31] A. Lühr and A. Saenz, Phys. Rev. A **81**, 010701(R) (2010).
[32] A. Igarashi and L. Gulyás, J. Phys. B: At. Mol. Opt. Phys. **51**, 035201 (2018).
[33] I. B. Abdurakhmanov, J. J. Bailey, A. S. Kadyrov, and I. Bray, Phys. Rev. A **97**, 032707 (2018).
[34] K. H. Spicer, C. T. Plowman, I. B. Abdurakhmanov, A. S. Kadyrov, I. Bray, and S. U. Alladustov, Phys. Rev. A **104**, 032818 (2021).
[35] K. H. Spicer, C. T. Plowman, I. B. Abdurakhmanov, S. U. Alladustov, I. Bray, and A. S. Kadyrov, Phys. Rev. A **104**, 052815 (2021).
[36] I. B. Abdurakhmanov, A. S. Kadyrov, and I. Bray, Phys. Rev. A **94**, 022703 (2016).
[37] I. B. Abdurakhmanov, C. T. Plowman, K. H. Spicer, I. Bray, and A. S. Kadyrov, Phys. Rev. A **104**, 042820 (2021).
[38] C. T. Plowman, I. B. Abdurakhmanov, I. Bray, and A. S. Kadyrov, Eur. Phys. J. D **76**, 31 (2022).
[39] C. T. Plowman, I. B. Abdurakhmanov, I. Bray, and A. S. Kadyrov, Eur. Phys. J. D **76**, 129 (2022).
[40] I. B. Abdurakhmanov, A. S. Kadyrov, and I. Bray, J. Phys. B: At. Mol. Opt. Phys. **49**, 03LT01 (2016).
[41] C. T. Plowman, K. H. Spicer, I. B. Abdurakhmanov, A. S. Kadyrov, and I. Bray, Phys. Rev. A **102**, 052810 (2020).
[42] S. U. Alladustov, I. B. Abdurakhmanov, A. S. Kadyrov, I. Bray, and K. Bartschat, Phys. Rev. A **99**, 052706 (2019).
[43] A. S. Kadyrov, J. J. Bailey, I. Bray, and A. T. Stelbovics, Phys. Rev. A **89**, 012706 (2014).
[44] A. S. Kadyrov, I. Bray, A. M. Mukhamedzhanov, and A. T. Stelbovics, Ann. Phys. (NY) **324**, 1516 (2009).
[45] W. L. Anderson, ACM Trans. Math. Softw. **8**, 344 (1982).
[46] K. H. Spicer, C. T. Plowman, S. U. Alladustov, I. B. Abdurakhmanov, I. Bray, and A. S. Kadyrov, Eur. Phys. J. D **77**, 131 (2023).
[47] K. H. Spicer, C. T. Plowman, M. Schulz, and A. S. Kadyrov, Phys. Rev. A **108**, 022803 (2023).
[48] L. H. Thomas, Proc. R. Soc. Lond. **114**, 561 (1927).
[49] M. Schulz, A. C. Laforge, K. N. Egodapitiya, J. S. Alexander, A. Hasan, M. F. Ciappina, A. C. Roy, R. Dey, A. Samolov, and A. L. Godunov, Phys. Rev. A **81**, 052705 (2010).
[50] A. Silvus, M. Dhital, S. Bastola, J. Buxton, Z. Klok, E. Ali, M. Ciappina, B. Boggs, D. Cikota, D. Madison *et al.*, J. Phys. B: At. Mol. Opt. Phys. **52**, 125202 (2019).